

Apparatus for Magnetization and Efficient Demagnetization of Soft Magnetic Materials

Paul Oxley

Physics Department, The College of the Holy Cross, Worcester, MA 01610 USA

This paper describes an electrical circuit that can be used to automatically magnetize and ac-demagnetize moderately soft magnetic materials and with minor modifications could be used to demagnetize harder magnetic materials and magnetic geological samples. The circuit is straightforward to replicate, easy to use, and low in cost. Independent control of the demagnetizing current frequency, amplitude, and duration is available. The paper describes the circuit operation in detail and shows that it can demagnetize a link-shaped specimen of 430FR stainless steel with 100% efficiency. Measurements of the demagnetization efficiency of the specimen with different ac-demagnetization frequencies are interpreted using eddy-current theory. The experimental results agree closely with the theoretical predictions.

Index Terms—Demagnetization, demagnetizer, eddy currents, magnetic measurements, magnetization, residual magnetization.

I. INTRODUCTION

THERE is a widespread need for a convenient and economical apparatus that can ac-demagnetize magnetic materials. It is well known that to accurately measure the magnetic properties of a material, it must first be in a demagnetized state. For this reason, measurements of magnetization curves and hysteresis loops use unmagnetized materials [1], [2] and it is thought that imprecise demagnetization is a leading cause for variations in the measured dc magnetic properties of soft ferromagnets [3]. Demagnetizing materials is also important for a range of other applications from demagnetizing steel architectural components [4] to demagnetizing mu-metal used in magnetically shielded rooms [5], [6]. Electromagnets wound on a magnetic material that are used to change between different magnetic fields must have the magnetic material fully demagnetized before changing the field. If not, the final field will not be determined solely by the current in the electromagnet coils, but also by the residual magnetism in the material produced by the previous field. There are also applications in the field of geology where soft magnetic material in rock samples is ac-demagnetized at frequencies of several hundred Hertz in order to measure the properties of the hard magnetic material also present [7].

The standard procedure to demagnetize a material is to apply a magnetic field with a direction that changes back and forth while at the same time the field amplitude reduces to zero. Electrical circuits that are designed to automatically produce an oscillating electrical current of diminishing amplitude can be used to generate such a magnetic field and here we describe such a circuit. The amplitude of the oscillating current produced by our circuit decreases linearly with time since this is the simplest decrease to implement. Other, more complicated time variations have been proposed [8] but in our tests we find the linear decrease in amplitude sufficient for full demagnetization of our sample. In addition to demagnetizing, our circuit can be used

to magnetize a magnetic sample by delivering a current proportional to an input voltage provided by the user and can be used to measure magnetic properties such as B - H hysteresis loops and magnetic permeability.

Our apparatus is simple, easy to use, and economical. It uses up-to-date electronic components, unlike many previous designs [9]–[13], which therefore tend to be rather complicated. More recent designs for demagnetization electronics exist but these do not provide sufficient information for another researcher to easily reproduce the demagnetization apparatus [14] or require substantial computer-controlled equipment and custom-written software to control the demagnetization cycle [15], [16]. Simply connecting a computer-controlled DAC to a programmable power supply is an alternative way to produce a decreasing amplitude sine wave current [17]. This solution also requires a PC and custom-written software, and would be significantly more expensive than our system. The finite voltage and time resolution of a DAC also limit the accuracy of the demagnetization waveform, especially towards the end of the demagnetization cycle when the current is small. In our apparatus the demagnetizing current frequency, amplitude, and duration can be controlled easily by adjusting potentiometers. The demagnetizing waveform is fully analogue and the demagnetization cycle can be initiated manually by the push of a button or automatically by a CMOS compatible voltage pulse.

Below, we describe our circuit in sufficient detail to allow others to replicate our design. Upon request, we can provide an electronic printed circuit board file that is ready to submit to a circuit board manufacturer. This would mean that minimal effort would be required to replicate our design. We also describe experiments to investigate how the amplitude, duration, and frequency of the demagnetizing field affect the demagnetization efficiency, as defined by (5). We find that 100% efficiency is possible and that the variation of efficiency with demagnetizing field frequency agrees closely with the theoretical prediction.

II. CIRCUIT DESCRIPTION

The circuit consists of two main parts: a voltage to current converter (V/I) circuit (Fig. 1) that provides a current proportional to an input voltage, and a demagnetizing circuit that pro-

Manuscript received February 01, 2009; revised April 03, 2009. Current version published August 19, 2009. Corresponding author: P. Oxley (e-mail: poxley@holycross.edu).

Color versions of one or more of the figures in this paper are available online at <http://ieeexplore.ieee.org>.

Digital Object Identifier 10.1109/TMAG.2009.2020795

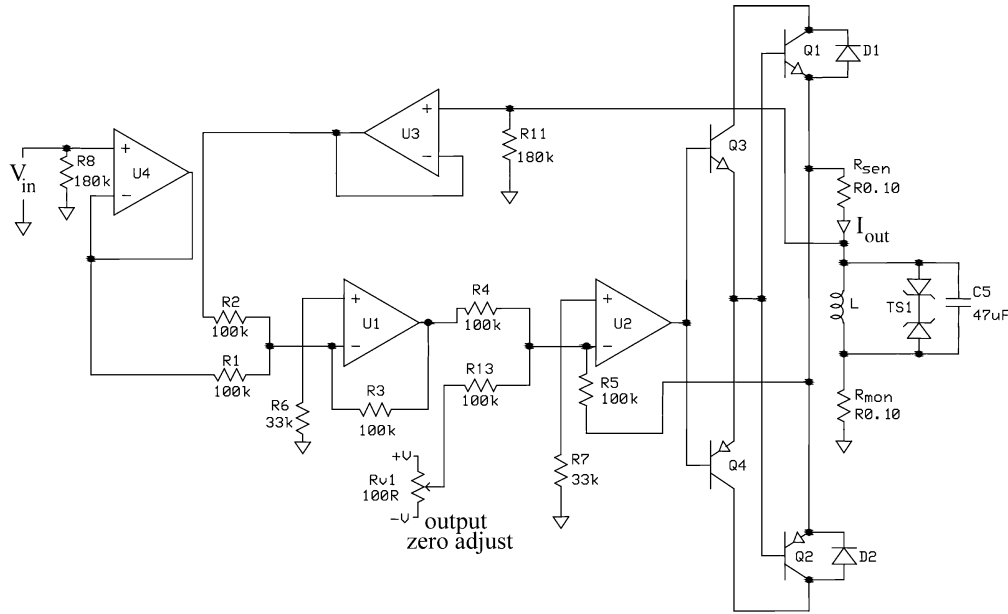


Fig. 1. Voltage to current converter (V/I) takes an input voltage, V_{in} , and produces an output current, I_{out} related to one another by (1). The current is passed through a coil, L , inside of which is placed the magnetic sample that is to be magnetized or demagnetized. The maximum delivered current depends on the voltage rating of the op amps and the current rating of the output transistors, respectively (20 V and 12 A for this work).

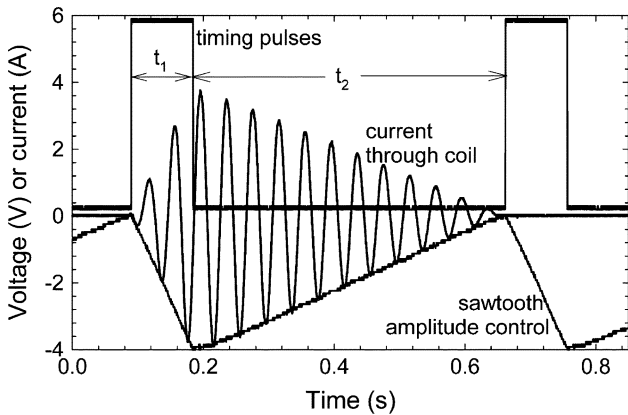


Fig. 2. Sinusoidal current waveform with variable amplitude can be used to demagnetize a magnetic sample inside the coil L in Fig. 1. This current waveform is generated when a similar voltage waveform, produced by the demagnetizing circuit, is fed to the input of the V/I circuit. The amplitude of the sine waveform is controlled by a saw-tooth waveform with rise and fall times (t_1 and t_2) determined by the timing pulses. Demagnetization takes place during the time t_2 .

duces a sine wave voltage of diminishing amplitude (Fig. 2). The demagnetizer circuit itself can be divided into three parts: a sine waveform generator circuit (Fig. 3), a saw-tooth waveform generator circuit (Fig. 4), and a control logic circuit (Fig. 5). Below, we describe these parts in detail.

A. V/I Circuit

The voltage-to-current converter shown in Fig. 1 produces a current, I_{out} , through a coil, L , which encloses the material we wish to magnetize or demagnetize. The current is proportional

to a voltage input, V_{in} , and is given by (1). The circuit is adapted from [18]

$$I_{out} = \frac{V_{in}}{R_{sen}}. \tag{1}$$

The circuit is highly stable and has a voltage-to-current characteristic that we have measured to be linear to 0.7%.

Resistor R_{v1} enables the current I_{out} to be zeroed when $V_{in} = 0$ V, allowing for any imbalance between the output of transistors Q1 and Q2. The transient suppressor, TS1, clamps the output voltage to a safe level in the event of any high voltage induced electromotive forces (EMFs) generated by the coil L . The capacitor C_5 acts as a noise suppressor and, since it is in parallel with L , allows the coil to operate in a resonant mode at the frequency $1/2\pi LC_5$ (neglecting the coil resistance). This reduces the current delivered by the transistors, whilst maintaining a higher current through the coil. The increase in current through the coil is small, however, unless the resistance of the coil is low ($<0.5 \Omega$), and was not significant in our studies.

B. Demagnetizer Circuit

The demagnetizer circuit produces a sinusoidal voltage with linearly decreasing amplitude, which is passed to the V/I circuit to generate the demagnetizing current, shown in Fig. 2. Timing pulses control the time (t_1) it takes for the sinusoidal current to ramp up to its maximum value, and the time (t_2) for the current to reduce to zero. It is during time t_2 when demagnetization takes place. The actual value of time t_1 is unimportant and is kept small to reduce power dissipation.

The heart of the demagnetizer circuit is the Exar XR2206 Monolithic Function Generator IC [19]. This circuit is capable of producing high quality sine, square, triangle, ramp, and pulse waveforms of high stability and accuracy. When generating a

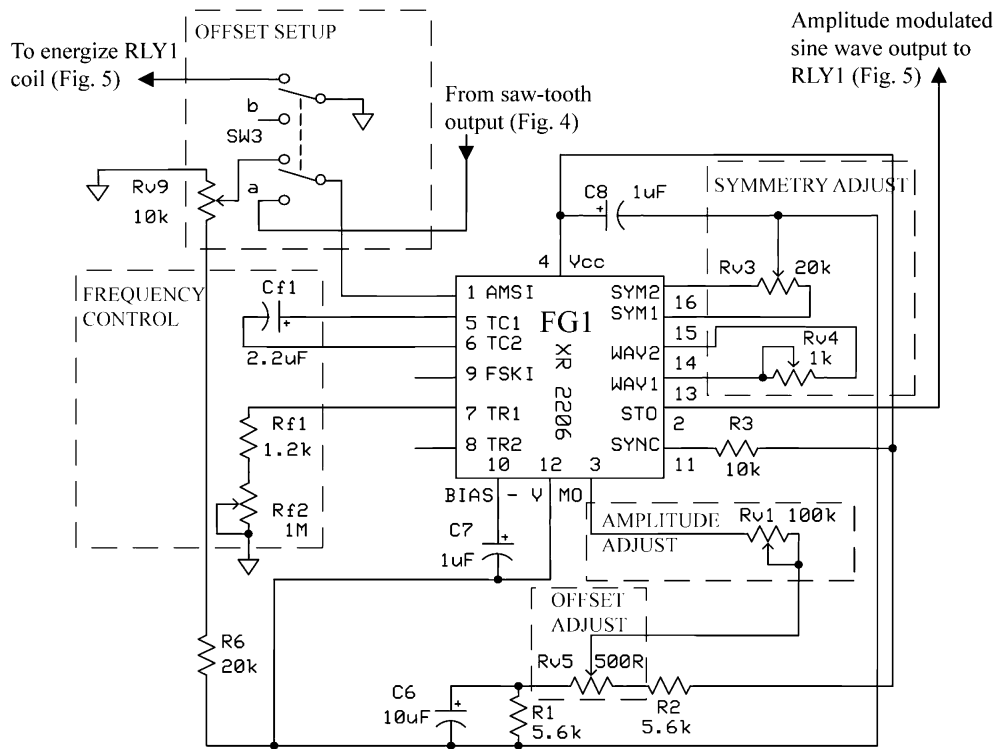


Fig. 3. Part of the demagnetizing circuit that produces a sinusoidal voltage with controllable amplitude and frequency. The amplitude is controlled by the voltage at pin 1 of FG1 up to a maximum amplitude set by R_{V1} . The frequency is determined according to (2). The symmetry adjust potentiometers R_{V3} and R_{V4} allow one to reduce contributions from higher harmonics of the fundamental sinusoidal frequency. When the offset setup switch SW3 is in the up position the offset adjust resistor R_{V5} allows one to easily and accurately ensure that the positive and negative amplitudes of the current waveform are equal.

sine wave we have experimentally found that all harmonics can be reduced to less than -40 dB of the amplitude of the fundamental frequency by adjusting the symmetry control on the XR2206 (see below). Importantly the sine waveform can be amplitude modulated by applying a control voltage to one of its inputs. This function is essential for producing a sinusoidal demagnetizing waveform that reduces linearly from its maximum amplitude to zero. The demagnetizing circuit uses two XR2206 integrated circuits. The first, FG1 in Fig. 3, produces a sinusoidal voltage, the amplitude of which is controlled by a saw-tooth waveform generated by a second, FG2 in Fig. 4. Control logic allows the demagnetization cycle to be initiated manually or automatically (Fig. 5). Below we provide more details of the operation of the circuits shown in Figs. 3–5.

Fig. 3 shows the circuit containing FG1 that produces a sinusoidal voltage with controllable frequency and amplitude. The frequency of the sine waveform is determined by capacitor C_{f1} and the resistors R_{f1} and R_{f2} and is given in (2)

$$f_0 = \frac{1}{C_{f1}(R_{f1} + R_{f2})}. \quad (2)$$

The capacitance can be in the range $0.001 \mu\text{F}$ to $100 \mu\text{F}$ and the total resistance range is $1 \text{ k}\Omega$ to $2 \text{ M}\Omega$. For the nominal component values shown in Fig. 3 the frequency range is 0.5 Hz to 380 Hz .

The maximum amplitude of the sine waveform is set by R_{V1} with a sensitivity of $60 \text{ mV/k}\Omega$. The actual amplitude of the

waveform at any time is controlled by the voltage applied to the AMSI input at pin 1. When the voltage at pin 1 is zero volts the amplitude of the output is zero volts. If the voltage at pin 1 is changed linearly to either $\pm 4 \text{ V}$ the output voltage changes linearly to the maximum amplitude that has been set by the amplitude control potentiometer R_{V1} . The only difference between the positive and negative control voltages is the phase of the output waveform. For our application either positive or negative control voltage suffices.

The harmonic content of the sinusoidal output can easily be reduced to less than 0.5% by the symmetry adjustment potentiometers R_{V3} and R_{V4} . The adjustment is as follows.

- 1) Set R_{V3} to its midpoint and adjust R_{V4} for minimum distortion.
- 2) With R_{V4} set as above, adjust R_{V3} to further reduce distortion.

The offset setup and offset adjust parts of the circuit are used to optimize the demagnetizing current waveform and are described below.

Fig. 4 shows the circuit containing FG2 that produces a saw-tooth voltage waveform that is used to control the amplitude of the sine waveform generated in Fig. 3. The circuit in Fig. 4 also produces the timing pulses that control the rise and fall times of the saw-tooth waveform. The frequency-shift keying (FSK) facility of the XR2206 IC enables the saw-tooth and timing pulses to be generated. Depending upon the voltage at the FSK input (pin 9), one of the two sets of timing resistors are chosen. When the FSK input is connected to the square wave SYNC output

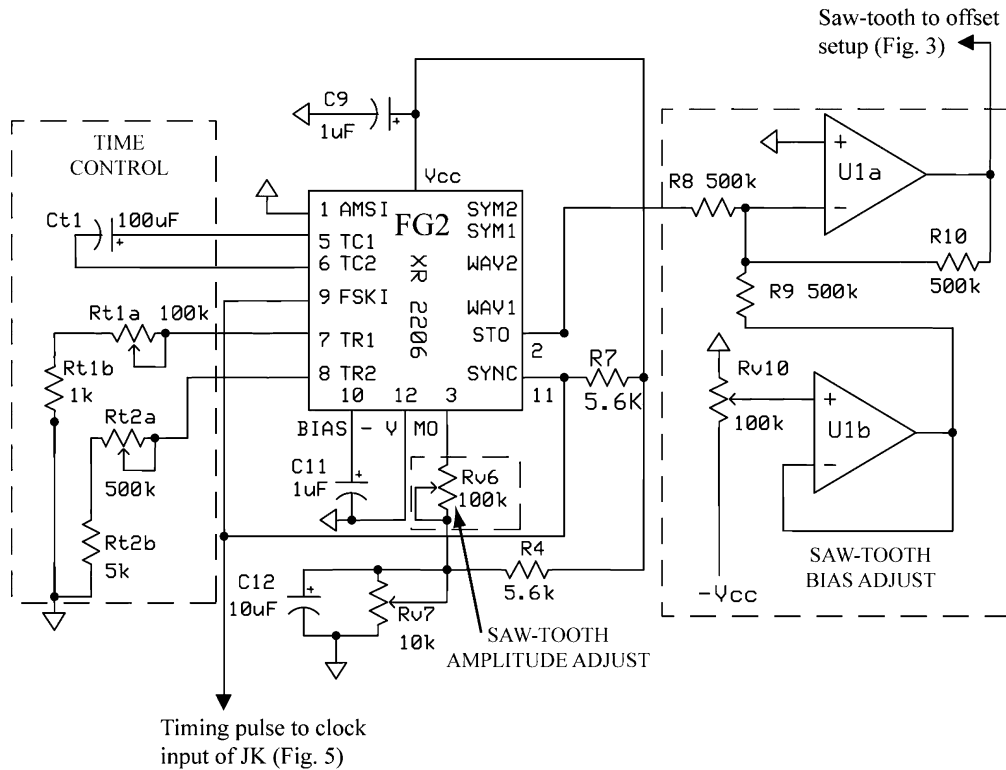


Fig. 4. Part of the demagnetizing circuit that generates the saw-tooth waveform used to control the amplitude of the sinusoidal waveform produced by FG1 in Fig. 3. The time control section determines the rise and fall times of the saw-tooth given by (3) and (4). The saw-tooth bias adjust allows the saw-tooth to be biased correctly before being applied to the amplitude control input (pin 1) of the sine wave generator FG1. The potentiometer R_{V6} is adjusted to provide a saw-tooth amplitude of 4 V required by FG1.

(pin 11), the circuit automatically frequency-shift keys between these two sets of timing resistors generating a saw-tooth waveform with different rise and fall times. The rise time, t_1 , is given by (3) and the fall time, t_2 , is given by (4)

$$t_1 = C_{t1}(R_{t1a} + R_{t1b})/2 \quad (3)$$

$$t_2 = C_{t1}(R_{t2a} + R_{t2b})/2. \quad (4)$$

For the circuit values shown, the rise and fall times are in the range 50 ms to 5 s, and 250 ms to 25 s, respectively. The saw-tooth waveform output at pin 2 is biased about $0.5 V_{cc}$, or +6 V, but to correctly control the amplitude of the sine waveform from FG1 the saw-tooth must be biased such that it has a maximum value of 0 V (the voltage is therefore always negative, see Fig. 2). The bias adjust circuit allows this to be done. The amplitude of the saw-tooth can be set to the required 4 V using potentiometer R_{V6} .

The sinusoidal waveform with the saw-tooth amplitude is generated repeatedly. The control logic circuit shown in Fig. 5 allows only one cycle to be passed to the V/I circuit by energizing the output relay (Relay 1) for one cycle, in synchronism with the timing pulses. The passing of the single cycle is initiated either manually by a push switch (SW5), or automatically by a voltage pulse applied to the “automatic demag.” input. When not demagnetizing, a voltage applied to the “magnetize” input is passed to the V/I circuit via a normally closed contact on Relay 1. This voltage provides V_{in} shown in Fig. 1 and can be

used to magnetize the sample enclosed within the coil L . When a signal to demagnetize is given, the rising edge of the next timing pulse energizes the relay to connect one cycle of the demagnetizing waveform to the input of the V/I circuit. At the end of the demagnetizing cycle, the relay is de-energized. Fig. 15 shows a full circuit diagram.

Only one adjustment is needed to produce a demagnetizing waveform that can efficiently demagnetize. This adjustment is made with switch SW3 in Fig. 3 placed in the “up” position. Then the amplitude modulation control voltage to pin 1 of FG1 is isolated from the saw-tooth generator. Instead, pin 1 is connected to potentiometer R_{V9} that allows the amplitude of the sine wave output to be adjusted to around 20 mV, simulating the voltages expected across the current monitoring resistor, R_{mon} , towards the end of a demagnetizing cycle. At the same time, the output relay is energized allowing the output current waveform to be viewed on an oscilloscope. The offset potentiometer R_{V5} in Fig. 3 can then be adjusted until the positive and negative amplitudes of the current waveform are exactly equal. In this way we can typically reduce the dc current offset to less than 1 mA, which is small enough to allow 100% demagnetization efficiency. Switch SW3 can then be placed in the “down” position ready for demagnetizing. This setup procedure is very quick and is only required if one changes the maximum demagnetization current amplitude. For our application, it is not envisioned that this current amplitude will be adjusted once the optimum maximum amplitude has been determined. Therefore, this set up procedure need only be carried out once.

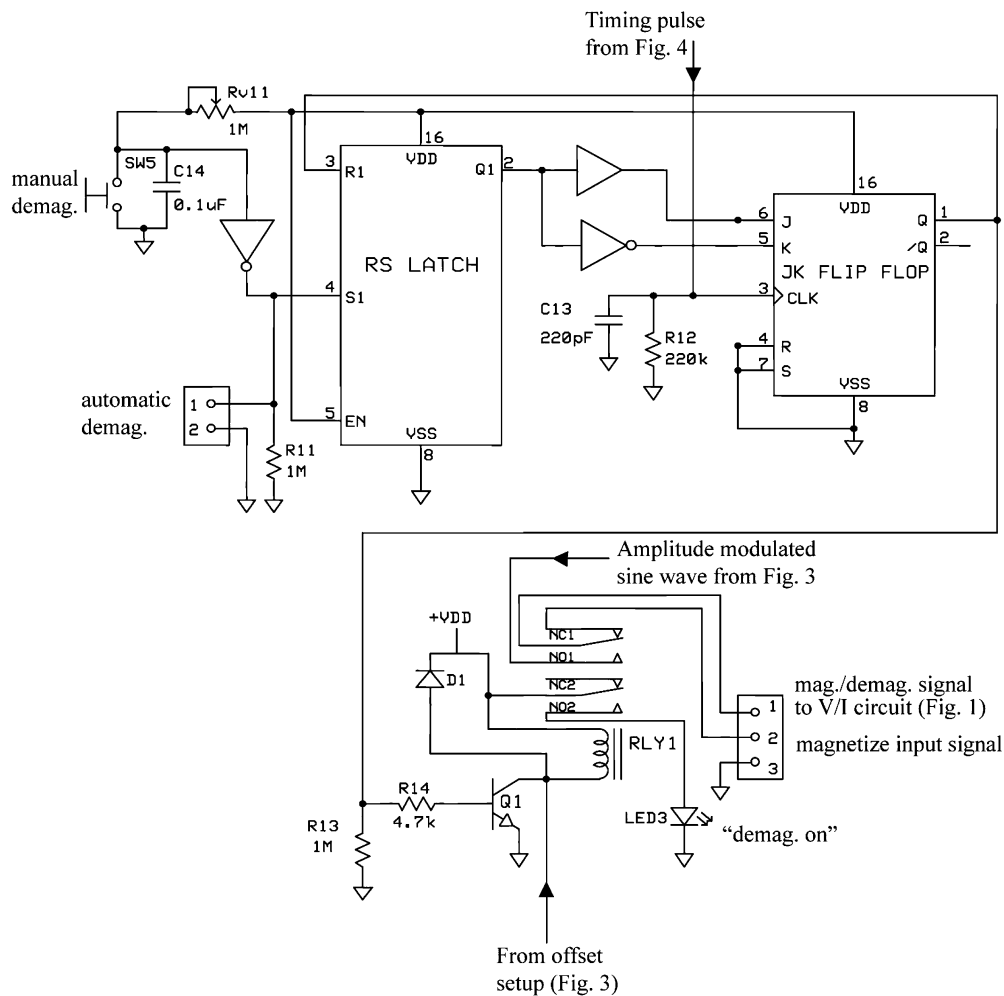


Fig. 5. Control logic circuit is used to allow only one cycle of the saw-tooth amplitude-controlled sinusoidal waveform to be passed to the V/I circuit. This circuit also allows either manual triggering of a demagnetization cycle via switch SW5, or automatic triggering when a CMOS compatible voltage pulse is applied. All logic components are 4000 series CMOS components.

The amplitude of the last half cycle of the demagnetizing current waveform is typically less than 10 mA and the current noise measured by a Keithley 2700 data acquisition system was found to be 0.2 mA, independent of current magnitude. No glitches or spikes in voltage or current were observed when the magnetizing coil was detached from the circuit. Such transients could have a detrimental effect on the demagnetization state of the sample and on circuit operation.

III. CIRCUIT PERFORMANCE AND RESULTS

A. Experimental Apparatus

To gauge the performance of our circuit, it was used to magnetize and demagnetize an electromagnet formed by winding a coil around a link-shaped magnetic specimen (Fig. 6). The specimen material is type 430FR magnetic stainless steel with circular cross section, and has a 1 mm slot in it at one point around the circumference. A magnetizing coil with 1700 turns/m of copper wire is wound tightly around the specimen. A Hall probe can be inserted into the slot to measure the magnetic flux density there, and a flux coil of 50 turns is wound on the specimen at a location opposite the slot. The Hall probe has a flux density

resolution of 0.1 G and to exclude the effect of the earth's magnetic field the probe was zeroed prior to taking measurements. By measuring the EMF induced in the flux coil we can determine the change in magnetic flux density, B , in the specimen. We cannot measure the magnetic field, H , directly, but it can be inferred from a measurement of the current through the coil in the following way. The coercive force of a straight rod of 430FR steel magnetized by a 4 Hz oscillating field to a maximum flux density of 1.0 T has previously been measured to be 265 A/m [20]. For our 430FR link-shaped specimen a 4 Hz current with amplitude 1.95 A produced a maximum flux density of 1.0 T, as measured by the flux coil. A measurement of the current and the flux density in the slot as a function of time showed that a flux density of zero was obtained at a current of -0.35 A. Therefore, a conversion factor of $265/0.35 = 760$ A/m per Amp is used to convert the measured current through the coil to a magnetic field. This linear conversion is only approximate due to the magnetic poles that reside in the specimen at either side of the slot.

B. Experimental Tests

To investigate how well magnetic flux in the specimen can be removed two different methods were employed to measure the

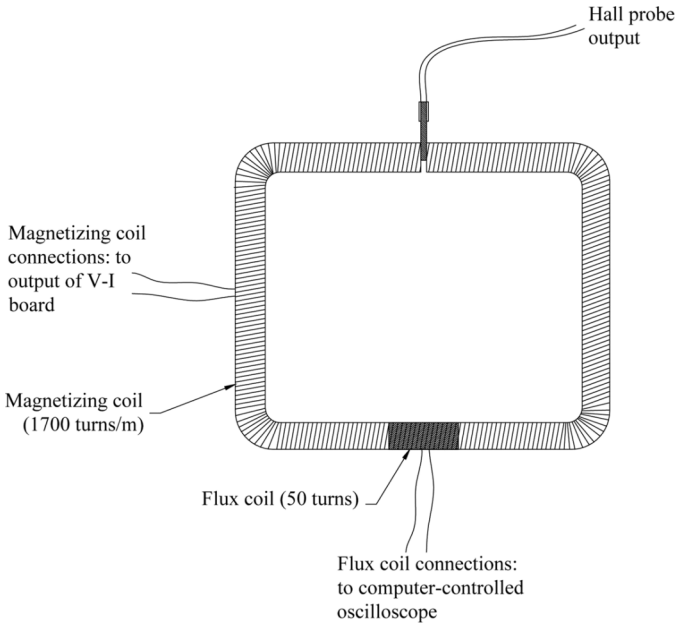


Fig. 6. Experimental apparatus used to perform the tests of our demagnetizing electronics. A link-shaped specimen made from 0.281-in diameter type 430FR magnetic stainless steel has a 1 mm slot. Into this slot is inserted a Hall probe, which is used to measure the magnetic flux density in the slot. The specimen has a magnetizing coil with approximately 1700 turns/m wound on it. A current passed through this coil, generated by the circuit described in this paper, is used to magnetize and demagnetize the specimen. When a changing current is passed through the magnetizing coil the EMF induced in the flux coil is used to measure the change in magnetic flux inside the steel. The flux coil is connected to an oscilloscope, which is under computer control to simplify data taking.

flux density. The first was simply to use the reading of the Hall probe located in the slot. We refer to this as the slot method. In the second method (the step method) a step in the current to the magnetizing coil was applied, which was sufficient to drive the specimen well into saturation, independent of its initial state of magnetization. The step current was created by feeding a voltage step from a synthesizer to the “magnetize” input in Fig. 5. The current step applied was from 0 A to +9 A in a time of 5 ms and the EMF induced in the flux coil was integrated to infer the change in magnetic flux density between the initial magnetization state and positive saturation. From this change in flux density the initial flux density in the specimen can be determined, as illustrated schematically in Fig. 7.

To determine how efficient the demagnetizing cycle was the specimen was first magnetized and the residual flux density, B_{mag} , was measured using both the slot method and the step method. The specimen was then magnetized again and subsequently demagnetized by a demagnetizing cycle from our circuit. The residual flux density, B_{demag} , was then measured using both the slot and the step methods. The efficiency of demagnetization, η , is defined as a percentage by (5)

$$\eta = 100 \times \left(1 - \frac{B_{demag}}{B_{mag}} \right). \quad (5)$$

In order to illustrate the performance of the demagnetizing electronics we performed three tests. In each test the specimen was first magnetized by a 5 A dc current. Measurements of the

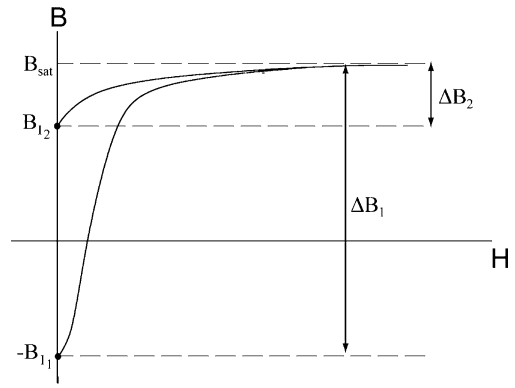


Fig. 7. Step method can be used to determine the flux density in our specimen. Two possible initial flux densities are shown ($B_{1,1}$ and $B_{1,2}$) and if the saturation flux density, B_{sat} , is known these initial flux densities can be measured in the following way. A large current step is applied to take the material to positive saturation independent of the initial flux density in the material. Integrating the EMF induced in the flux coil after this step change in current allows one to determine the change in flux density ($\Delta B_{1,2}$) and hence calculate the initial flux density from $B_{1,2} = B_{sat} - \Delta B_{1,2}$.

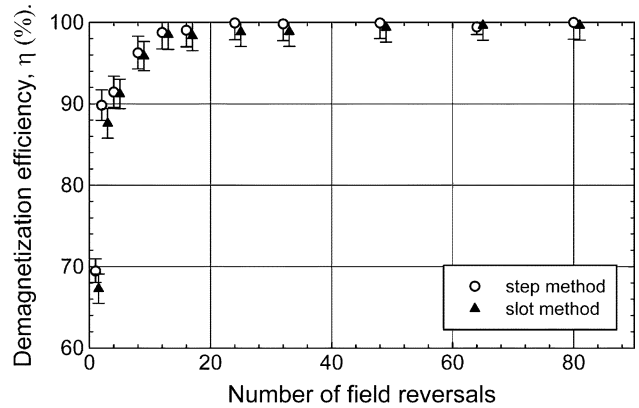


Fig. 8. Variation of the demagnetization efficiency with the number of field reversals during a demagnetization cycle for the 430FR specimen. For clarity the data for the slot method is shifted right by one reversal. The specimen was initially magnetized to saturation and then a 2 Hz, 460 A/m maximum amplitude demagnetizing cycle of variable duration was applied. Only two reversals are needed to remove the majority of the initial magnetization, but greater than 25 reversals are need for complete demagnetization.

flux density in the specimen for various magnetizing currents showed that 5 A was sufficient to bring the specimen to saturation. At saturation the actual field in the specimen is equal to the applied field, which for a current of 5 A is 8.5 kA/m.

In the first test the specimen was magnetized by the 5 A dc current, which was then removed and a 2 Hz, 460 A/m (0.6 A) maximum amplitude demagnetizing cycle was initiated. The duration of the demagnetizing cycle was varied from 0.25 s to 20 s corresponding to between one and eighty field reversals. Fig. 8 shows how the efficiency of demagnetization depended on the number of field reversals present during the cycle. One can see that there is very good agreement between the measured efficiencies for the slot and the step methods and the observed increase in efficiency with number of reversals is expected. We find that with only two reversals the efficiency is already quite high, about 90%, suggesting that the initial reversals are the most important for removing the bulk of the initial flux density,

but later reversals are clearly necessary for complete demagnetization. Greater than 25 reversals, which at 2 Hz take 6.25 s to complete, provides a demagnetization efficiency that is essentially 100%.

The second test investigated how the demagnetization efficiency depended on the magnitude of the applied demagnetizing field. The specimen was again magnetized to saturation by a 5 A dc current. This current was removed and a 100 Hz, variable amplitude demagnetizing cycle was initiated. The cycle duration was 0.5 s during which time the specimen experienced 100 field reversals. The variation of demagnetization efficiency with magnetic field is shown in Fig. 9. Again there is excellent agreement between the results using the slot method and the step method. A demagnetization field amplitude of 380 A/m was sufficient to fully demagnetize the specimen and we found that a dc field of -380 A/m produced a flux density in the slot equal in magnitude but opposite in direction to that remaining after a 5 A dc magnetization. Therefore we find that the minimum magnetic field needed for efficient demagnetization is equal to the field required to completely reverse the direction of the flux density. Minimizing the field required for full demagnetization is important for minimizing power loss during the demagnetization cycle.

For the final test we investigated how the demagnetization efficiency depended on the frequency of the demagnetizing field. The specimen was magnetized by a 5 A dc current and then demagnetized with a 460 A/m field of variable frequency in the range 2 Hz to 420 Hz. The duration of the demagnetizing cycle was varied with frequency so that roughly the same number of reversals were experienced at each frequency. The number of reversals at each frequency was between 100 and 125 for all frequencies except 1 Hz, which had 40 reversals, and 420 Hz, which had 210 reversals. The data are shown in Fig. 10. Again the slot and step methods are in excellent agreement and a reasonably high demagnetization efficiency (88%) is observed even at a frequency as high as 420 Hz. A reduction in the demagnetization efficiency with increased frequency is expected since eddy currents circulate in the material and shield the interior of the specimen from the applied magnetic field. This effect is investigated theoretically in Section III-C.

C. Eddy Current Theory

Higher frequencies of applied field induce larger eddy currents, which provide greater magnetic field shielding. A theoretical formulation of this effect is now given in order to compare to our experimental results in Fig. 10. In an infinitely long solid cylinder with a field applied parallel to the cylindrical axis the field inside the material, $H(r, t)$, satisfies the diffusion-type equation given in (6)

$$\frac{\partial^2 H(r, t)}{\partial r^2} + \frac{1}{r} \frac{\partial H(r, t)}{\partial r} = \frac{\mu_0 \mu_r}{\rho} \frac{\partial H(r, t)}{\partial t} \quad (6)$$

where r is the distance from the axis of the rod, μ_r is the relative permeability of the material that is assumed to be constant, and ρ is its electrical resistivity. The term on the right-hand side

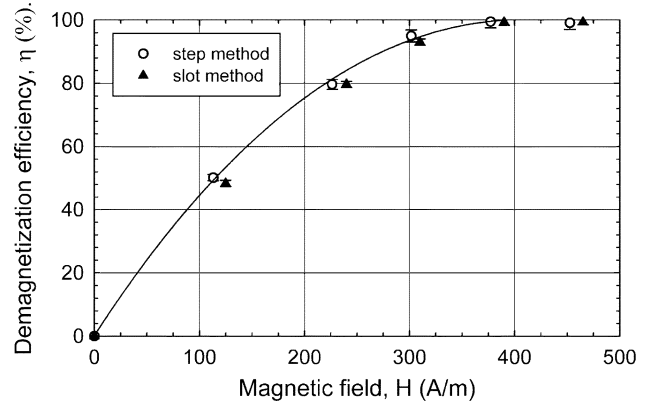


Fig. 9. Variation of the demagnetization efficiency with demagnetizing magnetic field amplitude for the 430FR specimen. For clarity the data for the slot method is shifted slightly higher in field. The specimen was initially magnetized to saturation and then a 100 Hz demagnetizing field with variable initial amplitude was applied for 100 reversals. A minimum field of 380 A/m was necessary for complete demagnetization. This field is just sufficient to completely reverse the direction of the initial flux density in the material. The solid line is a cubic fit to the step data and will be used in Section III-C.

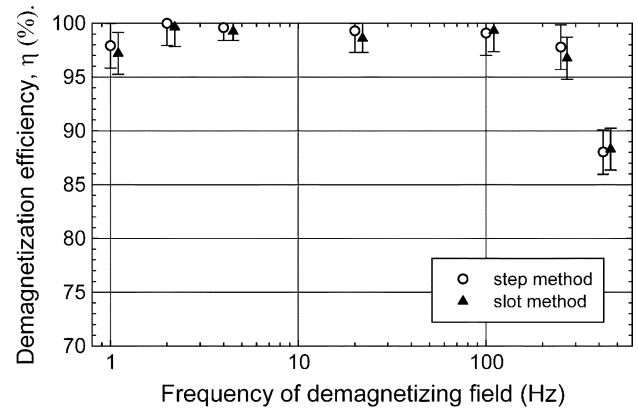


Fig. 10. Variation of the demagnetization efficiency with frequency of the demagnetizing field for the 430FR specimen. For clarity the data for the slot method are shifted slightly higher in frequency than those of the step method. The specimen was initially magnetized to saturation and then a variable frequency, 460 A/m amplitude demagnetizing field was applied for at least 40 reversals. High demagnetization efficiency (88%) is possible at a frequency as high as 420 Hz, despite eddy current shielding. The flux density remaining after demagnetization at 420 Hz was in the same direction as the initial magnetization.

of (6) originates from the induced EMF in the rod caused by a changing magnetic flux, and gives rise to the eddy currents. For a sinusoidal applied field of frequency $\omega/2\pi$ the solution to (6) is of the form $H(r, t) = H(r)e^{j\omega t}$ and (6) becomes the zeroth order Bessel's equation given in (7)

$$\frac{d^2 H(r)}{dr^2} + \frac{1}{r} \frac{dH(r)}{dr} - \frac{j\omega\mu_0\mu_r}{\rho} H(r) = 0. \quad (7)$$

The solution to (7) involves the Kelvin Functions $\text{Ber}(x)$ and $\text{Bei}(x)$ and is given in (8)

$$\frac{H(r)}{H_0} = \frac{\text{Ber}(\alpha r) + j\text{Bei}(\alpha r)}{\text{Ber}(\alpha r_0) + j\text{Bei}(\alpha r_0)} \quad (8)$$

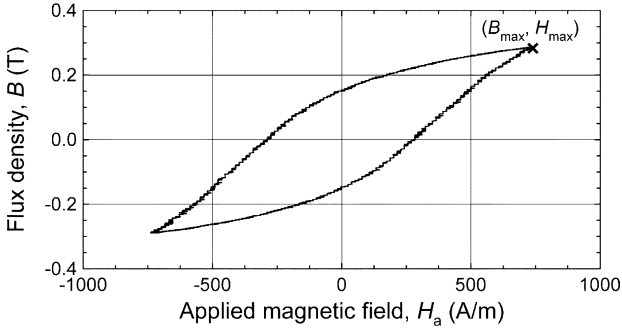


Fig. 11. Hysteresis loop used to determine the effective permeability of the 430FR specimen. The ratio of the maximum flux density to the maximum applied field at the tip of the loop gives the effective permeability, according to (11).

where H_0 is the field at the surface of the cylinder of radius r_0 , and $\alpha = \sqrt{\mu_0 \mu_r \omega / \rho}$. The Kelvin functions are given in (9)

$$\begin{aligned} \text{Ber}(x) &= \sum_{n=0}^{\infty} \frac{1}{[(2n)!]^2} \left(\frac{x}{2}\right)^{4n} (-1)^n \\ \text{Bei}(x) &= \sum_{n=0}^{\infty} \frac{1}{[(2n+1)!]^2} \left(\frac{x}{2}\right)^{4n+2} (-1)^n. \end{aligned} \quad (9)$$

The fraction of the surface field at a given position r is given in (10)

$$\left| \frac{H(r)}{H_0} \right| = \sqrt{\frac{\text{Ber}^2(\alpha r) + \text{Bei}^2(\alpha r)}{\text{Ber}^2(\alpha r_0) + \text{Bei}^2(\alpha r_0)}}. \quad (10)$$

Equation (10), along with the definition of α , applies to an infinite cylindrical rod, or equally well to a complete magnetic loop. For a specimen containing a slot however, the flux density is lower than that in a complete loop due to the presence of magnetic poles at the ends of the specimen next to the slot. The flux density is lower by a factor of μ_{eff}/μ_r , where μ_{eff} is the effective permeability, given by (11)

$$\mu_{\text{eff}} = \frac{B}{\mu_0 H_a} = \frac{B}{\mu_0 n I} \quad (11)$$

where H_a is the applied magnetic field, and n the number of turns per meter in the magnetizing coil (1700 for our specimen). The reduction in flux density, and therefore in eddy currents, due to the slot can then be accounted for by using μ_{eff} instead of μ_r on the right-hand side of (6) and in the definition of α

$$\alpha = \sqrt{\mu_0 \mu_{\text{eff}} \omega / \rho}. \quad (12)$$

The effective permeability was straightforward to determine experimentally. A 4 Hz sinusoidal current was passed through the magnetization coil wound on the specimen by feeding the signal from a synthesizer to the “magnetize” input in Fig. 5. The EMF induced in the flux coil was then integrated to infer the change in flux density during this cycle. The flux density

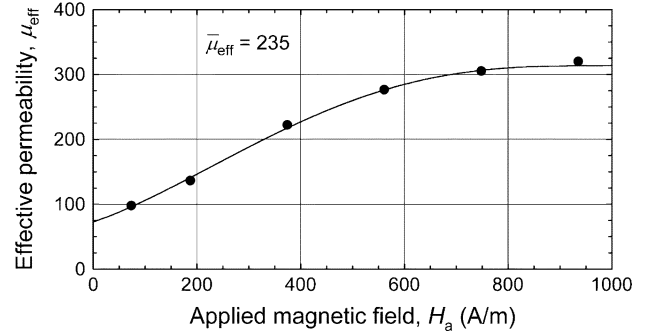


Fig. 12. Variation of effective permeability with applied magnetic field, $H_a = nI$, for the range of applied fields used when taking the data shown in Figs. 8–10. The solid line is a fourth order polynomial fit used to determine an average effective permeability, $\bar{\mu}_{\text{eff}}$, of 235. This value is used in (12) and (10) to determine the theoretical variation of magnetic field inside the specimen.

can then be plotted against the applied field to produce the hysteresis loop, as shown in Fig. 11. By using different current and therefore applied field amplitudes, the tips of the loops produced allowed us to determine the effective permeability, Fig. 12. The range of applied fields in Fig. 12 is the same range of fields used when taking the data shown in Figs. 8–10. The average effective permeability is 235 and this value can be used in (12) and (10) to determine the variation of magnetic field inside our specimen.

Since we know experimentally how the demagnetization efficiency, η , varies with magnetic field (solid line, Fig. 9) and we now know in theory how the magnetic field varies with position inside the specimen (10) we can deduce the expected variation of η inside the specimen, $\eta(r)$. This is shown in Fig. 13 for an applied field of frequency 420 Hz and a resistivity value of $7.6 \times 10^{-7} \Omega \cdot \text{m}$ for 430FR stainless steel [21]. The average demagnetization efficiency over the cross-sectional area, $\bar{\eta}$, is defined as

$$\bar{\eta} = \frac{1}{\pi r_0^2} \int_0^{r_0} \eta(r) 2\pi r dr. \quad (13)$$

The theoretical value of $\bar{\eta} = 86\%$ derived from Fig. 13 is in close agreement with the experimentally determined value of 88% demagnetization efficiency at 420 Hz.

IV. CIRCUIT PERFORMANCE USING SOLENOIDS

The above results illustrate the ability of our circuit to completely demagnetize a magnetic specimen by passing a current through a coil wound directly on the specimen. An alternative situation of placing a sample that one wishes to demagnetize inside a solenoid would be useful for demagnetizing straight magnetic rods and geological samples. Here, we provide a brief theoretical guide as to the performance of our circuit when used in this configuration.

When demagnetizing samples the most important consideration is the maximum attainable magnetic field. The maximum magnetic field that can be generated in a solenoid connected to our circuit is determined by the solenoid impedance in

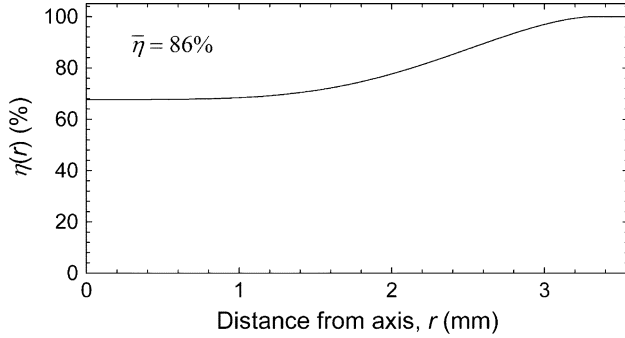


Fig. 13. Variation of demagnetization efficiency, η , with distance, r , from the symmetry axis of the specimen. The curve combines the experimental variation $\eta(H)$ from Fig. 9, solid line, and the theoretical prediction for the variation $H(r)$ in (10). In (10) a permeability of 235 and an electrical resistivity of $7.8 \times 10^{-7} \Omega\cdot\text{m}$ are used. The demagnetization efficiency is lower near the axis due to eddy current shielding of the applied demagnetizing field. The average efficiency over the cross sectional area of the specimen, $\bar{\eta}$, is 86%, in good agreement with the experimental value of 88% (Fig. 10).

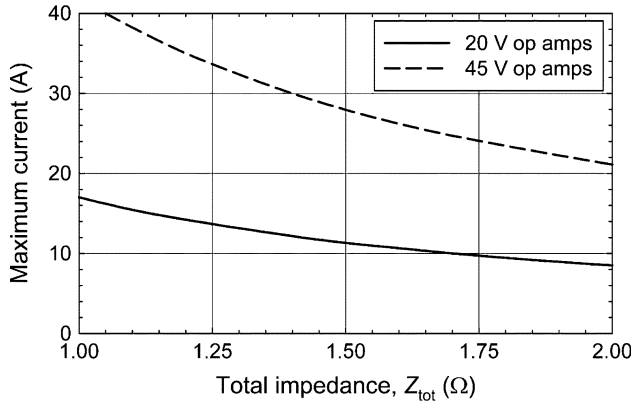


Fig. 14. Maximum current that can be provided by our circuit depends on the total impedance seen by the circuit. The total impedance includes the impedance of the coil in series with the sense and monitor resistors (both 0.10Ω). Two theoretical curves are shown, one when using op amps rated at 20 V (as in this work) and one with 45 V op amps, which could be used instead to provide higher current.

series with the sense and monitor resistors R_{sen} and R_{mon} (both 0.10Ω). The total impedance is given by (14)

$$Z_{\text{tot}} = R_{\text{sen}} + R_{\text{mon}} + R + j\omega L \quad (14)$$

where $\omega = 2\pi f$ and f is the frequency of the alternating current in the solenoid (during demagnetization, for example) and R and L are the resistance and inductance of the solenoid. In general the inductive impedance of the solenoid depends on the magnetic sample placed inside. Since this is different for every sample we simply assume in (14) the impedance of an empty solenoid. We note though that [22] calculates the inductive impedance of a solenoid surrounding a magnetic core that could, along with a measurement of the phase lag between magnetic field and flux density, be used to take into account the effect of the magnetic sample.

The magnitude of the current passing through the solenoid is given by (15)

$$I = \frac{V_o - V_t}{|Z_{\text{tot}}|} = \frac{V_o - V_t}{\sqrt{(R + R_{\text{sen}} + R_{\text{mon}})^2 + \omega^2 L^2}} \quad (15)$$

where V_o is the voltage rating of the op amps U1, U2, U3, and U4 in Fig. 1, and V_t is the saturation voltage drop across the transistors Q1 and Q2, which was 3 V for the transistors used here. Fig. 14 shows how the current through the solenoid varies with the total impedance, Z_{tot} , for two different values of V_o : 20 V as used in our apparatus, and 45 V, which can be obtained using higher voltage op amps (e.g., OPA445AP). Since the magnetic field inside the solenoid is proportional to the current, the maximum attainable field is determined by the quantities V_o , R , ω , and L (assuming $V_t = 3$ V). Equation (16) gives the magnetic field, H , at the center of a solenoid of diameter d and length a , with n turns/m

$$H = \frac{naI}{\sqrt{d^2 + a^2}} = \frac{na(V_o - V_t)}{\sqrt{(d^2 + a^2)[(R + R_{\text{sen}} + R_{\text{mon}})^2 + \omega^2 L^2]}} \quad (16)$$

As an example a 20 cm long solenoid with diameter 3 cm wound with three layers of 1 mm diameter wire carrying a 1 Hz current has a total impedance of 1.4Ω . From (15), or Fig. 14, a maximum current of 12 A could be obtained using 20 V op amps and a current of 30 A using 45 V op amps. Equation (16) predicts magnetic fields at the center of the solenoid of 3.5×10^4 A/m and 9×10^4 A/m for the two current values.

V. CONCLUSION

We have constructed and tested an electronic apparatus that can be used to magnetize and demagnetize magnetic specimens. The circuit has been shown to demagnetize with 100% efficiency a link-shaped specimen constructed of magnetic stainless steel. The tests performed using our circuit demonstrate the circuit abilities and give results that are consistent with eddy current theory. A more comprehensive comparison between theory and experiment could be undertaken in the future. By choosing higher voltage and current components our circuit can generate larger magnetic fields suitable for demagnetizing harder magnetic materials or geological samples, and we have given a theoretical analysis of the circuit's performance for such an application.

APPENDIX

See Fig. 15.

ACKNOWLEDGMENT

The author wishes to thank J. Oxley for technical expertise throughout this work, D. Miller for machining expertise used in constructing parts of the experimental setup, and Dr. D.-P. Yang for useful discussions and for reading the manuscript. The

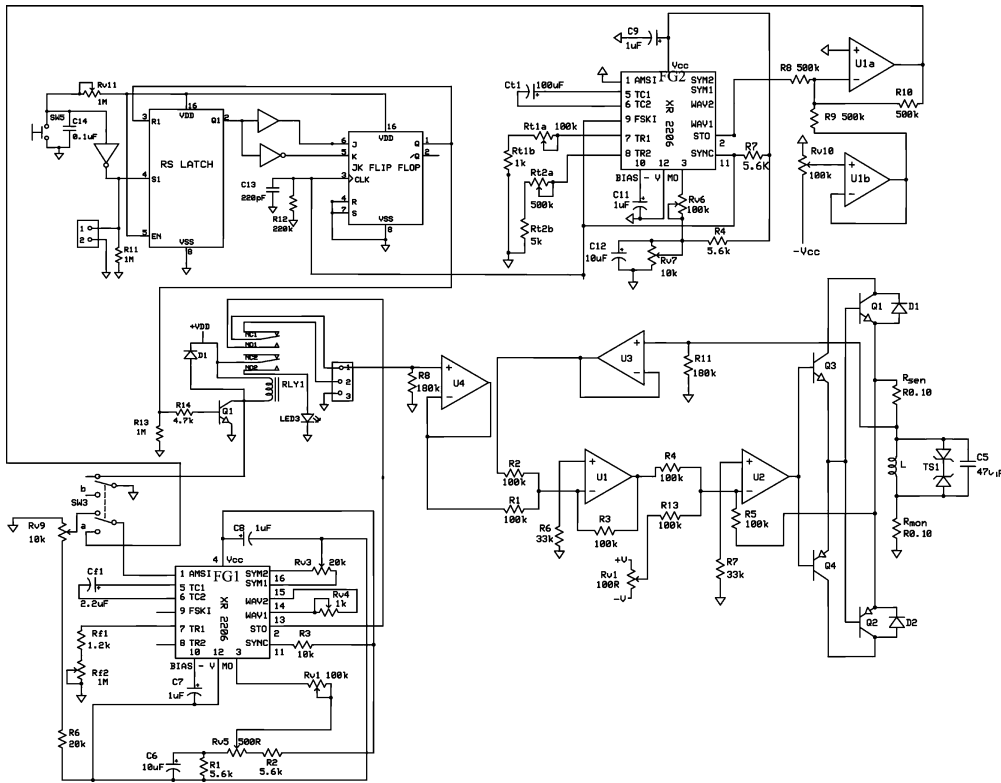


Fig. 15. Entire circuit layout indicating how the four circuits shown in Figs. 1, 3, 4, and 5 connect together.

author thanks the referees for their helpful comments. This work was supported by the Research Corporation through a Cottrell College Science Award and by the College of the Holy Cross through a Research and Publication Award.

REFERENCES

[1] G. Hilton, S. A. Eccleston, and A. G. Clegg, "Improving accuracy of intrinsic coercivity measurements for magnetically soft materials," *IEEE Trans. Magn.*, vol. 41, no. 8, pp. 2322–2327, Aug. 2005.
 [2] S. Takahashi *et al.*, "Analysis of minor hysteresis loops for neutron radiation and plastic deformation in pure Fe," *IEEE Trans. Magn.*, vol. 43, no. 6, pp. 2689–2691, Jun. 2007.
 [3] R. M. Strnat, M. J. Hall, and M. S. Masteller, "Precision and accuracy study on measurement of soft magnetic properties using dc hysteresis-graphs," *IEEE Trans. Magn.*, vol. 43, no. 5, pp. 1884–1887, May 2007.
 [4] K. Yamazaki *et al.*, "Investigation on demagnetization of residual magnetization in architectural components using 3-D magnetic field analysis," *IEEE Trans. Magn.*, vol. 41, no. 5, pp. 1976–1979, May 2005.
 [5] F. Thiel, A. Schnabel, S. Knappe-Gruneberg, D. Stollfuß, and M. Burghoff, "Demagnetization of magnetically shielded rooms," *Rev. Sci. Instrum.*, vol. 78, p. 035106, 2007.
 [6] S. Knappe-Gruneberg, A. Schnabel, G. Wuebbeler, and M. Burghoff, "Influence of demagnetization coil configuration on residual field in an extremely magnetically shielded room: Model and measurements," *J. Appl. Phys.*, vol. 103, p. 07E925, 2008.
 [7] A. Hayashida, K. L. Verosub, F. Heider, and R. Leonhardt, "Magnetostigraphy and relative palaeointensity of late Neogene sediments at ODP leg 167 site 1010 off Baja California," *Geophys. J. Int.*, vol. 139, pp. 829–840, 1999.
 [8] F. Thiel, A. Schnabel, S. Knappe-Gruneberg, D. Stollfuß, and M. Burghoff, "Proposal of a demagnetizing function," *IEEE Trans. Magn.*, vol. 43, no. 6, pp. 2959–2961, Jun. 2007.
 [9] R. A. Newbury, "Demagnetizer for solid specimens," *J. Phys. E*, vol. 2, pp. 315–318, 1969.

[10] A. de Sa and J. W. Widdowson, "A digitally controlled AF demagnetizer for peak fields of up to 0.1 T," *J. Phys. E*, vol. 8, pp. 302–304, 1975.
 [11] K. Mohri, "An accurate ac demagnetizing method using a linear inductance for high permeability cores," *IEEE Trans. Magn.*, vol. MAG-12, no. 4, pp. 385–389, Jul. 1976.
 [12] K. Karunakar, M. Ranjan, and K. S. Prabhu, "A low-cost demagnetizer with controllable cycle and adjustable level," *IEEE Trans. Magn.*, vol. MAG-17, no. 5, pp. 2488–2492, Sep. 1981.
 [13] D. C. Jiles, D. L. Atherton, H. E. Lassen, D. Noble, J. de Vette, and T. Astle, "Microcomputer-based system for control of applied uniaxial stress and magnetic field," *Rev. Sci. Instrum.*, vol. 55, pp. 1843–1848, 1984.
 [14] C.-J. Juan, C.-C. Kuo, and C.-Y. Wen, "The study and implementation of a microprocessor-controlled demagnetizer," *IEEE Trans. Consum. Electron.*, vol. 44, no. 2, pp. 405–412, May 1998.
 [15] A. Shahvaroghi and A. J. Moses, "High-speed computerised dc magnetisation and demagnetisation of mild steel," *J. Magn. Magn. Mater.*, vol. 133, pp. 386–389, 1994.
 [16] V. F. Matyuk and A. A. Osipov, "A setup for measuring the magnetic characteristics of soft magnetic materials and articles," *Russ. J. Nondestruct. Test.*, vol. 43, pp. 143–153, 2007.
 [17] P. Anderson, "A universal dc characterisation system for hard and soft magnetic materials," *J. Magn. Magn. Mater.*, vol. 320, pp. e589–e593, 2008.
 [18] M. Frantisek, "V/I converter accommodates grounded load," *Electron. Des. News*, 10th ed. Jun. 1999, p. 120.
 [19] Exar Corporation, [Online]. Available: <http://www.exar.com>
 [20] P. Oxley, J. Goodell, and R. Molt, "Magnetic properties of stainless steels at room and cryogenic temperatures," *J. Magn. Magn. Mater.*, vol. 321, no. 14, pp. 2107–2114, Jul. 2009.
 [21] D. W. Dietrich, "Magnetically soft materials," in *ASM Handbook*. Materials Park, OH: ASM, 1990, vol. 2.
 [22] M. C. Rodriguez and C. Sanz, "Simple frequency domain model for hysteresis and eddy currents in cylindrical and parallelepipedal cores," *IEEE Trans. Magn.*, vol. 43, no. 5, pp. 1912–1919, May 2007.